Shengna Liu, Xiaochuan Liu and Liancun Zheng*

Boundary Layer Mechanism of a Two-Phase Nanofluid Subject to Coupled Interface Dynamics of Fluid/Film

https://doi.org/10.1515/zna-2019-0171 Received May 21, 2019; accepted August 25, 2019; previously published online September 20, 2019

Abstract: This article investigates boundary layer mechanism of a two-phase nanofluid over a thin liquid film of power-law fluid. We take the coupled interface dynamics between the thin liquid film and nanofluid into consideration, where the thermal conductivity and dynamic viscosity are assumed to be linear functions of nanoparticle concentration. The influence of Brownian motion and thermophoresis of the nanofluid is also considered. Numerical results are carried out by employing similarity transformation and byp4c technique. The heat and mass transfer in the flow boundary layer are analysed by relevant parameters with the assistance of graphs. The results show that heat conduction decreases significantly with the increase of rheological properties parameter and tensile velocity ratio. Rheological properties parameter, tensile velocity ratio, Brownian motion parameter and thermophoresis parameter play important roles in mass transfer.

Keywords: Brownian Motion; Heat and Mass Transfer; Interface Dynamics; Nanofluid; Thin Liquid Film.

1 Introduction

Fluid flow induced by the motion of the stretching sheet is a common phenomenon occurring in many industrial settings such as extrusion, wire drawing, glass fibre, paper production, etc. [1–3]. In 1970, Crane [4] studied the steady two-dimensional incompressible boundary-layer flow of a Newtonian fluid caused by the linear stretching elastic sheet. Rajagopal et al. [5] investigated the flow of

*Corresponding author: Liancun Zheng, School of Mathematics and Physics, University of Science and Technology Beijing, Beijing 100083, China, E-mail: liancunzheng@ustb.edu.cn

Shengna Liu: School of Energy and Environmental Engineering, University of Science and Technology Beijing, Beijing 100083, China

Xiaochuan Liu: School of Mathematics and Physics, University of Science and Technology Beijing, Beijing 100083, China

an incompressible viscoelastic second-order fluid past a stretching sheet and concluded that skin-friction coefficient and the boundary layer velocity decreased with the increase of elastic parameter. Gorla et al. [6] analysed the steady three-dimensional boundary-layer flow of a powerlaw fluid over a linear stretching sheet and the influence of power-law index and stretching ratio on boundary layer velocity. Kumar et al. [7, 8] analysed magnetohydrodynamic (MHD) radiative nonaligned stagnation point motion of non-Newtonian liquid over a stretched surface and the boundary-layer flow of MHD fluid past a cone and a wedge with nonuniform heat source/sink along with Cattaneo-Christov heat flux. Magyari and Keller [9] studied the heat and mass transfer of the Newtonian fluid in the boundary layers on an exponentially stretching continuous surface. Kumar et al. [10] carried out a numerical study of MHD radiative micropolar liquid flow driven by stretching sheet and compared the velocity and temperature fields with or without slip. Liao [11] used the homotopy analysis method to investigate the series solution of unsteady boundary-layer flow on a stretching flat plate. Sajid and Hayat [12] presented the influence of thermal radiation on the boundary-layer flow of an exponentially stretched thin plate.

These studies were confined to ordinary Newtonian and non-Newtonian fluids, which have low heat transfer coefficients. However, adding nanoparticles to traditional fluids can significantly improve the thermal conductivity of fluids. Choi and Estman [13] were the first to name fluids containing nanoparticles as nanofluids, which can be synthesised by uniformly dispersing nanoparticles in the base liquids in a one- or two-step method [14]. And the use of nanofluids as coolants in heat exchangers, renewable energy sources transportations, microelectronics, chemical engineering, and aerospace and manufacturing has become more and more common [15–17]. Because of the high thermal conductivity of nanofluids, the knowledge of heat and mass transport of nanofluids driven by stretched sheets plays an important role in engineering, science, and technology. Many numerical and experimental results have shown that the two-phase models are more accurate than the single-phase models, and the pure fluid correlation tends to systematically underestimate the

heat transfer coefficient of nanofluids [18–20]. Thus, the two-phase models are usually used to research the flow, heat, and mass transfer of nanofluids. Buongiorno [21] explained the abnormal convective heat transfer enhancement observed in nanofluids and combined with Brownian diffusion and thermophoresis effects established a general two-component nonuniform equilibrium model of transport phenomena in nanofluids. Khan and Pop [22] investigated the boundary-layer flow of a nanofluid past a stretching sheet and obtained a similarity solution depending on the Prandtl number, Lewis number, Brownian motion number, and thermophoresis number. Noghrehabadi et al. [23] analysed the effects of partial slip boundary conditions on the flow and heat transfer of nanofluids over a stretching sheet at constant wall temperature. Kumar et al. [24] studied the effects of Brownian motion and thermophoresis on the bioconversion flow of nanoliquids over a variable thickness surface with slip effects and revealed the general flow field and density of moving microorganisms under different physical parameters. In 2015, Zargartalebi et al. [25] considered a problem to investigate stagnation-point flow of nanofluids over an isothermal stretching sheet; they assumed the thermal conductivity and dynamic viscosity of the nanofluids were linear functions of the volume fraction of nanoparticles when the volume fraction of nanoparticles was very small; the numerical solution was presented based on the finite difference method. Akbar et al. [26] numerically studied the magnetohydrodynamic transport of nanofluids on the surface of a vertical stretched plate with exponential temperature-dependent viscosity and buoyancy effects.

However, the above literatures ignored the coupling interface dynamics between the sheet and the fluid. Unlike the classic problem in those literatures, Al-Housseiny and Stone [27] first considered the coupling dynamics between the sheet and the fluid and obtained the self-similar solutions of boundary-layer flow for Newtonian fluids in 2012. In their article, two kinds of sheets were considered: an elastic sheet and a viscous sheet, considered as a Newtonian fluid. However, it is difficult to stretch Newtonian fluid in Newtonian fluid. Binding and Walters [28] estimated the extensional viscosity of polymer solutions by contraction flow experiments. Both grades of polyacrylamide (ElO and 1175, supplied by Allied Colloids Ltd) aqueous solutions were power-law stretching with high elasticity. A finite fluid medium, i.e. thin liquid film, has been more and more widely used in practical applications, such as the fresh paint and protective coating [29–31]. Sandeep and Malvandi [32] and Sandeep [33] studied the enhanced heat transfer of non-Newtonian nanofluids containing graphene nanoparticles in liquid film flow and the effect of aligned magnetic field on the flow of magnetic nanofluids containing graphene nanoparticles in liquid film. Meyer et al. [34] constructed an automated thin film stretcher for control over biomaterials via thin film stretching to generate anisotropic polymeric particles.

In this article, the boundary layer mechanism of two-phase nanofluids induced by power-law stretching of the thin liquid film is studied. Unlike the classic studies, in this article the coupled interface dynamics between the thin liquid film and nanofluids are taken into consideration. According to literatures [25, 35–37], if the volume fraction of the nanofluid is very small, then the thermal conductivity and dynamic viscosity are linear functions of the concentration of nanoparticles. The numerical solutions of nonlinear boundary layer equations are obtained by similarity transformation and the bvp4c function in MATLAB. The effects of relevant parameters on reduced skin-friction coefficient, Nusselt number, Sherwood number, boundary-layer flow, and heat and mass transfer are discussed in detail.

2 Physical Model

Here, we consider a film with uniform temperature distribution immersed in nanofluids, which stretches along the *x* axis to drive the flow of nanofluids. The flow takes place at y > h(x), where y is the coordinate measured normal to the stretching surface, h(x) is the vertical distance between the upper surface of the thin liquid film, and the x axis at the stretching distance x. The tensile velocity U(x)of thin liquid film varies with the value of x and at the inlet is U_0 ; when stretched to the distance L, the stretching speed is $U_L(U_L > U_0)$. The temperature and concentration T_w and C_w on the surface of the thin liquid film are kept constant, which were higher than the ambient temperature and concentration T_{∞} and C_{∞} , respectively. Supposing that the length of the thin film in the lateral direction is much larger than its thickness, we treat the problem as a two-dimensional dynamics system. The thin film and the surrounding nanofluid are in a steady state. A schematic diagram of the physical model is illustrated in Figure 1.

2.1 Formulation of Governing Equations

According to literature [21], we assume that nanoparticles are in local thermal equilibrium with the (Newton) base fluid, ignoring the viscous dissipation of nanofluids. The base fluid around the nanoparticles is regarded as a continuum. Brownian motion and thermophoresis are the most important factors that cause relative slip between

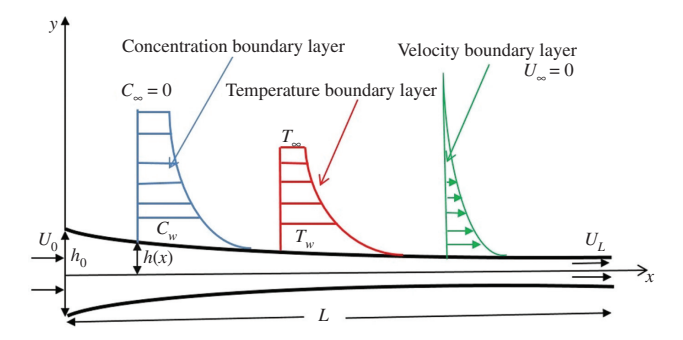


Figure 1: Schematic of a thin liquid film immersed in the nanofluid.

nanoparticles and the base fluid in the laminar sublayer near the thin film. Considering the influence of the volume fraction of nanoparticles in the base fluid less than 3% and the effects of Brownian motion and thermophoresis, the boundary layer–governing equations are written as follows [21, 25, 27]:

$$\frac{\partial u}{\partial x} + \frac{\partial v}{\partial y} = 0,\tag{1}$$

$$u\frac{\partial u}{\partial x} + v\frac{\partial u}{\partial y} = \frac{\mu_{nf,\infty}}{\rho_{nf}} \frac{\partial}{\partial y} \left(\frac{\mu_{nf}}{\mu_{nf,\infty}} (C) \frac{\partial u}{\partial y} \right), \tag{2}$$

$$u\frac{\partial T}{\partial x} + v\frac{\partial T}{\partial y} = \frac{k_{nf,\infty}}{(\rho c)_{nf}} \frac{\partial}{\partial y} \left(\frac{k_{nf}}{k_{nf,\infty}} (C) \frac{\partial T}{\partial y} \right)$$

$$+ \tau \left\{ D_B \frac{\partial C}{\partial y} \frac{\partial T}{\partial y} + \frac{D_T}{T_\infty} \left(\frac{\partial T}{\partial y} \right)^2 \right\}, \tag{3}$$

$$u\frac{\partial C}{\partial x} + v\frac{\partial C}{\partial y} = D_B \frac{\partial^2 C}{\partial y^2} + \frac{D_T}{T_\infty} \frac{\partial^2 T}{\partial y^2},\tag{4}$$

The corresponding boundary conditions are

$$y = h(x): u = U(x), \quad v = U(x)\frac{\mathrm{d}h}{\mathrm{d}x},$$

$$T = T_w, \quad C = C_w,$$
(5)

$$y \to +\infty$$
: $u = 0$, $T = T_{\infty}$, $C = C_{\infty}$, (6)

in which u and v are the velocity components in the x and y directions, respectively; ∞ and w are the ambient and surface conditions, respectively; C is the concentration of nanoparticles; μ_{nf} is the dynamic viscosity of the nanofluid; k_{nf} is the thermal conductivity of the nanofluid; ρ_{nf} is the density of the nanofluid; c_{nf} is the specific heat capacity of the nanofluid; D_B is the Brownian motion coefficient; D_T is the thermophoretic diffusion coefficient; h(x) is the half-thickness of the thin film; $\tau = (\rho c)_p/(\rho c)_{nf}$. Supposing that the thickness of the thin film changes very slowly, the velocity distribution of the thin film is uniform in the y direction. According to previous literature [25], when the volume fraction of nanoparticles in the

base fluid is less than 3% the thermal conductivity and dynamic viscosity of the nanofluid are linearly dependent on the volume fraction of the nanoparticles. The thermal conductivity and dynamic viscosity coefficients have the following linear relationships with the volume fraction of nanoparticles [25]:

$$\frac{\mu_{nf}}{\mu_{nf,\infty}} = 1 + N_{\nu} \frac{(C - C_{\infty})}{(C_{w} - C_{\infty})}, \quad \frac{k_{nf}}{k_{nf,\infty}} = 1 + N_{c} \frac{(C - C_{\infty})}{(C_{w} - C_{\infty})},$$
(7)

where N_v and N_c are the variable viscosity parameter and variable thermal conductivity parameter, respectively.

2.2 Interface Dynamics of the Thin Liquid Film

Next, we consider the interface dynamics of the thin liquid film. As the thin film is incompressible, it satisfies the continuity equation [27]:

$$h_0 U_0 = h(x) U(x) \tag{8}$$

The momentum balance equation of the thin film in the *x* direction can be written as [27]:

$$\frac{\partial \sigma_{xx}}{\partial x} + \frac{\partial \sigma_{yx}}{\partial y} = \rho_s U \frac{\mathrm{d}U}{\mathrm{d}x},\tag{9}$$

in which σ_{xx} is the normal stress; σ_{yx} is the sheer stress at the upper surface of the thin film. As the film is symmetrical around the x axis, the following formula can be obtained by integrating (9) from 0 to h(x) and introducing the expression $\tau_{yx} = \mu_{nf,w} \partial u/\partial y|_{y=h(x)}$ of the surface friction of thin liquid film in the x direction:

$$\frac{\mathrm{d}}{\mathrm{d}x}(h\sigma_{xx}) + \mu_{nf,w} \frac{\partial u}{\partial y}\bigg|_{y=h(x)} = \rho_s h U \frac{\mathrm{d}U}{\mathrm{d}x}$$
 (10)

Because the thin liquid film is power law stretched, according to the literature [28], we assume $\sigma_{xx} = \mu_{tf} (\mathrm{d}U/\mathrm{d}x)^m$. $\mu_{tf} (\mathrm{d}U/\mathrm{d}x)^{m-1}$ (m>1) is the extensional viscosity of the thin film; μ_{tf} is a constant, which assumed to be much larger than the viscosity of the surrounding nanofluid; m is the power-law index (i.e. rheological properties parameter). Substituting equation $\sigma_{xx} = \mu_{tf} (\mathrm{d}U/\mathrm{d}x)^m$ and the continuity (8) into (10), we get:

$$\frac{\mathrm{d}}{\mathrm{d}x} \left(\frac{\mu_{tf}}{U(x)} \left(\frac{\mathrm{d}U}{\mathrm{d}x} \right)^m - \rho_s U \right) + \frac{\mu_{nf,w}}{h_0 U_0} \frac{\partial u}{\partial y} \bigg|_{y=h(x)} = 0 \quad (11)$$

The ratio of the stretching force to the inertial force of the thin film is approximately equal to $\mu_{tf}U_0^{m-2}/\rho_sL^m$.

We assume that $\mu_{tf}U_0^{m-2}/\rho_sL^m$ is large enough to ignore the inertia force. Then, the formula (11) can be reduced as follows:

$$\frac{\mathrm{d}}{\mathrm{d}x} \left(\frac{\mu_{tf}}{U(x)} \left(\frac{\mathrm{d}U}{\mathrm{d}x} \right)^m \right) + \frac{\mu_{nf,w}}{h_0 U_0} \frac{\partial u}{\partial y} \bigg|_{y=h(x)} = 0 \tag{12}$$

3 Similarity Variable and Functions

We introduce the following dimensionless quantities [27]:

$$\eta = \frac{y - h(x)}{h_0 g(x)}, \quad u = U(x) f'(\eta), \tag{13}$$

$$v = -h_0 \frac{\mathrm{d}(gU)}{\mathrm{d}x} f(\eta) + U(x) \left(\frac{\mathrm{d}h}{\mathrm{d}x} + h_0 \eta \frac{\mathrm{d}g}{\mathrm{d}x} \right) f'(\eta), \quad (14)$$

$$T = (T_w - T_\infty)\theta(\eta) + T_\infty, \quad C = (C_w - C_\infty)\phi(\eta) + C_\infty,$$
(15)

The u and v automatically satisfy the continuity (1). Replacing the dimensionless quantities (13), (14), and (15) into (2), (3), and (4), respectively, we have

$$(1+N_{\nu}\phi)f''' + N_{\nu}f''\phi' + \left(\frac{\rho_{nf}(h_{0}g)^{2}U'}{\mu_{nf,\infty}} + \frac{\rho_{nf}h_{0}^{2}gUg'}{\mu_{nf,\infty}}\right)ff''$$
$$-\frac{U'\rho_{nf}(h_{0}g)^{2}}{\mu_{nf,\infty}}(f')^{2} = 0$$
(16)

$$(1 + N_c \phi)\theta'' + \left(N_c + \tau D_B \frac{(C_w - C_\infty)(\rho c)_{nf}}{k_{nf,\infty}}\right)\theta'\phi'$$

$$+ \frac{(\rho c)_{nf}h_0^2 g}{k_{nf,\infty}} \frac{d(gU)}{dx}\theta'f + \frac{\tau D_T (T_w - T_\infty)(\rho c)_{nf}}{T_\infty k_{nf,\infty}}(\theta')^2 = 0$$
(17)

$$\phi'' + \frac{D_T(T_W - T_\infty)}{D_B T_\infty(C_W - C_\infty)} \theta'' + \frac{h_0^2 g}{D_B} \frac{d(gU)}{dx} f \phi' = 0$$
 (18)

subject to the dimensionless boundary conditions:

$$\eta = 0: f'(0) = 1, \quad f(0) = 0, \quad \theta(0) = 1, \quad \phi(0) = 1$$
 $\eta \to +\infty: f'(\eta) \to 0, \quad \theta(\eta) \to 0, \quad \phi(\eta) \to 0$
(19)

In (16-18), g(x) and U(x) are unknown functions. In order to get the similarity solutions of (16-18), we must have

$$\frac{\rho_{nf}(h_0g(x))^2 U'(x)}{\mu_{nf,\infty}} = 1$$
 (20)

$$\frac{\rho_{nf}h_0^2g(x)U(x)g'(x)}{\mu_{nf,\infty}} = \beta \tag{21}$$

Among them, β is a constant determined by the dynamic coupling between the thin film and nanofluids.

According to (20) and (21), we can get the following formula:

$$\frac{\rho_{nf}(h_0g(x))^2 U'(x)}{\rho_{nf}h_0^2g(x)U(x)g'(x)} = \frac{1}{\beta}$$
 (22)

By integrating (22), we get

$$g(x) = \varepsilon U(x)^{\beta}, \tag{23}$$

here ε is the integral constant. By substituting (23) into (20), we have $\rho_{nf}h_0^2\varepsilon^2U(x)^{2\beta}\mathrm{d}U=\mu_{nf,\infty}\mathrm{d}x$. For $\beta=-1/2$, both g(x) and U(x) are exponential functions; otherwise, g(x) and U(x) are the power-law functions with the form $(Ax+B)^P$. The stretching speed of the thin film satisfies the boundary conditions: $U(0)=U_0$, $U(L)=U_L$. Then, for $\beta\neq-1/2$,

$$U(x) = U_0 \left(-t \frac{x}{L} + 1 \right)^{-\gamma}, \quad t = 1 - \left(\frac{U_0}{U_I} \right)^{\frac{1}{\gamma}},$$
 (24)

substituting (24) into (20), we get

$$g(x) = (\text{Re})^{-\frac{1}{2}} \left(-t \frac{x}{L} + 1 \right)^{-\gamma \beta}, \quad \gamma = -\frac{1}{1 + 2\beta},$$
 (25)

where Re = $t\gamma U_0 h_0^2 \rho_{nf}/\mu_{nf,\infty} L$ is the generalised Reynolds number.

Similarly, for $\beta = -1/2$,

$$U(x) = U_0 e^{\left(\frac{1}{L} \ln \frac{U_L}{U_0}\right)x}, \quad g(x) = \text{Re}^{-\frac{1}{2}} e^{-\left(\frac{1}{2L} \ln \frac{U_L}{U_0}\right)x},$$
 (26)

where $\text{Re} = \left(\rho_{nf} U_0 h_0^2 \ln(U_L/U_0) / \mu_{nf,\infty} L \right)$ is the generalised Reynolds number. The functions U(x) and g(x) should simultaneously satisfy the dynamic (12) of the thin film. On the surface of the thin film, we have $\left. \frac{\partial u}{\partial y} \right|_{y=h(x)} = \left(\frac{U(x)f''(0)}{h_0g(x)} \right)$, then (12) becomes

$$\frac{\mathrm{d}}{\mathrm{d}x} \left(\frac{\mu_{tf}}{U(x)} \left(\frac{\mathrm{d}U}{\mathrm{d}x} \right)^m \right) + \frac{\mu_{nf} U(x) f''(0)}{h_0^2 g(x) U_0} = 0 \qquad (27)$$

For $\beta \neq -1/2$, by substituting (24) and (25) into (27), we can get the following formula:

$$\gamma \beta - \gamma = -\gamma m - m + \gamma - 1 \tag{28}$$

As $\gamma = -1/(1+2\beta)$, we get $\beta = -3/(1+2m)$, $\gamma = (2m+1)/(5-2m)$. Then, the full similarity solutions of (2–4) are as follows:

$$(1+N_{\nu}\phi)f'''+N_{\nu}f''\phi'+\frac{2m-2}{2m+1}ff''-(f')^2=0, \quad (29)$$

$$(1 + N_c \phi)\theta'' + (N_c + N_b)\theta'\phi' + \Pr_{nf} \frac{2m - 2}{2m + 1} f\theta' + N_t(\theta')^2 = 0,$$
(30)

$$\phi'' + \frac{N_t}{N_h}\theta'' + Sc\frac{2m-2}{2m+1}f\phi' = 0,$$
 (31)

where primes denote differentiation with respect to η , and the four nondimensional parameters are defined by

$$N_b = au D_B rac{(C_W - C_\infty)(
ho c)_{nf}}{k_{nf,\infty}}, \quad N_t = au D_T rac{(T_W - T_\infty)(
ho c)_{nf}}{T_\infty k_{nf,\infty}},$$
 $\Pr_{nf} = rac{v_{nf,\infty}}{lpha_{nf,\infty}}, \quad Sc = rac{v_{nf,\infty}}{D_B},$

here $v_{nf,\infty} = \mu_{nf,\infty}/\rho_{nf}$ denotes kinematic viscosity of the nanofluids. Physical quantities of interest to us, namely, local Nusselt number Nu_x , local Sherwood number Sh_x , and local skin-friction coefficient C_{fx} , are defined as follows:

$$Nu_{x} = \frac{xq_{w}}{k_{nf,\infty}(T_{w} - T_{\infty})}, \quad Sh_{x} = \frac{xq_{m}}{D_{B}(C_{w} - C_{\infty})},$$

$$C_{fx} = \frac{2\tau_{nf,w}}{\rho_{nf}U^{2}(x)},$$
(32)

here quantities of surface heat flux q_w , surface mass flux q_m , and surface shear stress $\tau_{nf,w}$ are defined as follows:

$$q_{w} = -k_{nf,w} \left(\frac{\partial T}{\partial y}\right) \Big|_{y=h(x)}, \quad q_{m} = -D_{B} \left(\frac{\partial C}{\partial y}\right) \Big|_{y=h(x)},$$

$$\tau_{nf,w} = \mu_{nf,w} \left(\frac{\partial u}{\partial y}\right) \Big|_{y=h(x)}$$
(33)

Substituting (33) into (32) and using (13) and (15), the relationships between local Nusselt number, local skinfriction coefficient, local Sherwood number, and the generalised Revnolds number are obtained:

$$Nu_{x} \text{Re}^{-\frac{1}{2}} = -\frac{(1+N_{c})x\theta'(0)}{h_{0}} \left(-t\frac{x}{L}+1\right)^{\frac{3}{2m-5}},$$
 (34)

$$C_{fx} \operatorname{Re}^{\frac{1}{2}} = \frac{(4m+2)th_0 f''(0)}{(5-2m)L} (1+N_{\nu}) \left(-t\frac{x}{L}+1\right)^{\frac{2m-2}{5-2m}},$$
 (35)

$$Sh_x \text{Re}^{-\frac{1}{2}} = -\frac{x\phi'(0)}{h_0} \left(-t\frac{x}{L} + 1\right)^{\frac{3}{2m-5}},$$
 (36)

where $Nu_X \text{Re}^{-\frac{1}{2}}$, $C_{f_X} \text{Re}^{\frac{1}{2}}$, and $Sh_X \text{Re}^{-\frac{1}{2}}$ are the reduced Nusselt number (Nur), the reduced skin-friction coefficient (Cfr), and the reduced Sherwood number (Shr), respectively. In the same way, we can get that for $\beta = -1/2$; there are no full similarity solutions for (2-4).

When parameters m = 1, Nc = 0, Nb = 0, Nt = 0, (29) and (30) degenerate to $f''' - (f')^2 = 0$ and $\theta'' = 0$, respectively, from which we can see that, when the Newtonian fluid viscous sheet is stretched to drive the flow of Newtonian fluid, the flow has no effect on heat transfer, which is impossible. That is to say, the viscous plate of Newtonian fluid cannot drive the motion of Newtonian fluid by stretching.

4 Numerical Method and Verification

In order to solve the nonlinear coupled ordinary differential (29-31) with boundary conditions (19), the byp4c technique is adopted. We consider $f = f_1, f' = f_2, f'' = f_3, \theta =$ $f_4, \theta' = f_5, \phi = f_6$, and $\phi' = f_7$. Then, (29–31) are reduced into systems of first-order ordinary differential equations as follows:

$$\begin{split} f_{1}' &= f_{2}, \\ f_{2}' &= f_{3}, \\ f_{3}' &= (1 + Nvf_{6})^{-1} \left[(f_{2})^{2} - \frac{2m - 2}{2m + 1} f_{1}f_{3} - Nvf_{3}f_{7} \right], \\ f_{4}' &= f_{5}, \\ f_{5}' &= (1 + Ncf_{6})^{-1} \left[-(Nc + Nb)f_{5}f_{7} \right. \\ &- \Pr_{nf} \frac{2m - 2}{2m + 1} f_{1}f_{5} - Nt(f_{5})^{2} \right], \\ f_{6}' &= f_{7}, \\ f_{7}' &= -\frac{Nt}{Nb} (1 + Ncf_{6})^{-1} \left[-(Nc + Nb)f_{5}f_{7} \right. \\ &- \Pr_{nf} \frac{2m - 2}{2m + 1} f_{1}f_{5} - Nt(f_{5})^{2} \right] - Sc\frac{2m - 2}{2m + 1} f_{1}f_{7}, \end{split}$$

subject to the following initial conditions:

$$f_1(0) = 0$$
, $f_2(0) = 1$, $f_3(0) = -0.1$, $f_4(0) = 1$, etc.

We adopt the default value 10^{-3} of byp4c as relative error tolerance and choose a suitable finite value of $\eta \to \infty$, namely, $\eta = \eta_{\infty} = 25$.

If the volume fraction of nanoparticles is assumed to be zero and the thin liquid film is stretched linearly, (29) reduces to

$$f''' - (f')^2 = 0 (37)$$

with the boundary conditions:

$$f'(0) = 1, \quad f'(+\infty) = 0$$
 (38)

In literature [27], the analytic solution of formula (37) was given: $f'(\eta) = 6/(\eta + \sqrt{6})^2$.

From the expression of $f'(\eta)$, we can also get $f''(\eta) = -12/\left(\eta + \sqrt{6}\right)^3$.

In order to verify the accuracy of numerical solution, the comparison between numerical solution and analytical solution of (37) is shown in Figure 2. It can be seen that numerical solution is highly agreement with the analytical solution. At the same time, the numerical and analytical results of $f''(\eta)$ are compared in Table 1. The results show that their results are also highly consistent.

When Nc = Nv = Nb = Nt = Sc = 0, $Pr_{nf} = 1$, and $L/h_0 = 5$, Table 2 compares the results for the reduced Nusselt number and reduced skin-friction coefficient obtained in the present work with those reported by Liu et al. [38] for m = 1.2, m = 1.4, respectively. As can be seen

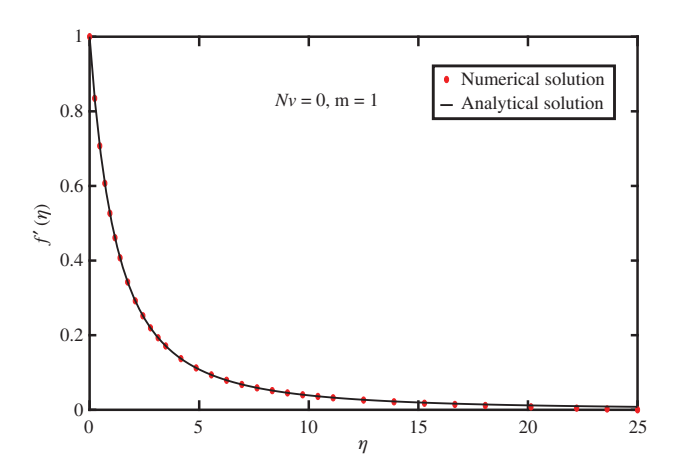


Figure 2: Comparison of the numerical solution and analytical solution of the momentum equation.

from Table 2, the current results are in good agreement with Liu and colleagues' [38].

5 Results and Discussion

Equations (29–31) consist of three related hydrodynamic variables (f', θ, ϕ) and seven parameters, namely, Nv, Nc, m, Nb, Nt, Pr_{nf} , and Sc. According to the expressions of Nv and Nc in literature [25]: $Nv = 1 - \mu_{bf}/\mu_{nf,\infty}$, Nc = $1 - k_{bf}/k_{nf,\infty}$, we get 0 < Nv, Nc < 1. The experimental studies in literatures [39-42] showed that the values of Nv and Nc were generally between 0 and 0.2. However, under hypothetical conditions, thermal conductivity of nanofluids can be increased by adding nanoparticles with larger thermal conductivity and smaller particle size or by increasing the temperature of nanofluids and the volume fraction of nanoparticles, thus making Nc larger. Nv can also be made larger by changing conditions. For example, Godson et al. [43] studied the thermal conductivity and viscosity of water-based silver nanofluids. When the volume fraction of nanoparticles was 0.9%, the ranges of Nv and Nc were 0.2-0.3 and 0.2-0.6 respectively, with changing of temperature. If we increase the volume fraction of silver nanoparticles to close to 3%, the values of Nv and *Nc* will be larger. Thus, we suppose that $0.2 \le Nv \le 0.6$ and $0.3 \le Nc \le 0.9$. The magnitude of *m* is determined by the rheological properties of the thin liquid film, where only the case of m > 1 is considered. For other parameters, we take $0.1 \le Nb$, $Nt \le 0.5$ [44, 45], $Pr_{nf} = 2.3$, and 1 < Sc < 10 [46].

Table 1: Comparisons between numerical and analytical solutions of $f''(\eta)$ at Nv=0, m=1.

η	0	2.083	4.861	7.639	10.42
Numerical solution $f''(\eta)$	-0.8165	-0.1289	-0.03074	-0.01175	-0.005764
Exact solution $f''(\eta)$	-0.8165	-0.1289	-0.0307	-0.0117	-0.0056

Table 2: Comparison of results for the reduced Nusselt number *Nur* and reduced skin-friction coefficient *Cfr* with drawing velocity ratio U_L/U_0 when Nc = Nv = Nb = Nt = Sc = 0, $Pr_{nf} = 1$, $L/h_0 = 5$.

U_L/U_0		m = 1.4	m=1.2		
	Nur (Liu et al. [38])	Nur (present results)	<i>Cfr</i> (Liu et al. [38])	Cfr (present results)	
1.5	1.55012	1.5501	-0.11119	-0.1112	
2.0	1.94536	1.9454	-0.16588	-0.1659	
2.5	2.32011	2.3201	-0.19785	-0.1978	
3.0	2.67929	2.6793	-0.21848	-0.2185	
3.5	3.02603	3.0260	-0.23267	-0.2327	
4.0	3.36245	3.3625	-0.24288	-0.2429	

5.1 Effects of Different Parameters on Fields of Velocity, Temperature, and Concentration

We can see from (29) that the velocity boundary layer is mainly affected by the variable viscosity parameter *Nv* and rheological properties parameter *m*. Figures 3 and 4 depict the variation of the velocity boundary layer under different variable viscosity parameter *Nv* and rheological properties parameter *m*. When other parameters are fixed, it is detected that the thickness of the velocity boundary layer increases slightly with the increase of the variable viscosity parameter *Nv* and decreases slightly with the increase of the rheological properties parameter *m*. This is because higher value of *Nv* enhances the viscosity of the nanofluids. Larger viscosity of fluids improves the fluidity and thus boosts the velocity distribution. However, the increase of rheological property parameter *m* lessens

the fluidity of fluid, resulting in the reduction of velocity boundary layer thickness.

Figures 5 and 6 indicate that the variable thermal conductivity parameter Nc of the nanofluid has a little effect, but the rheological properties parameter (power-law exponent m) of the thin film has great influence on temperature boundary layer. Higher value of Nc enhances the temperature boundary layer thickness; however, opposite behaviour is examined via larger m. This is because the thermal conductivity of nanofluids increases slightly with the increase of Nc and thus leads to the boost of temperature boundary layer thickness. The tensile viscosity of the thin film reduces by enhancing m, resulting in the change of fluidity of nanofluids and the decrease of velocity profile. On the one hand, the reduction of fluidity leads to the change of temperature boundary layer. On the other hand, larger values of rheological parameter *m* decay the heat exchange capacity between the film and nanofluids;

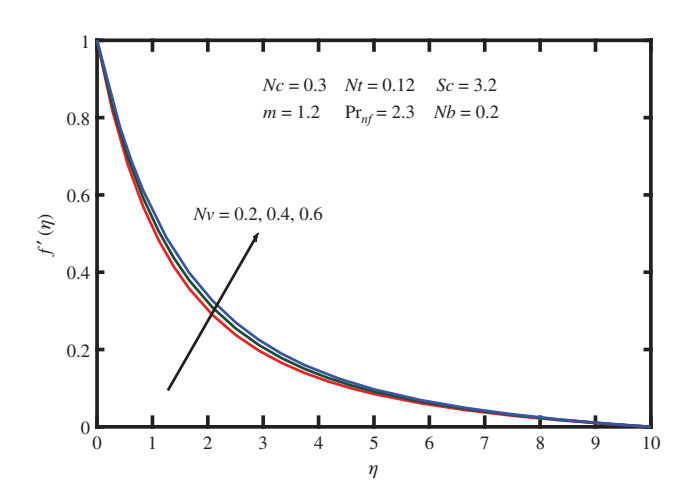


Figure 3: Velocity profiles for variable viscosity parameter Nv.

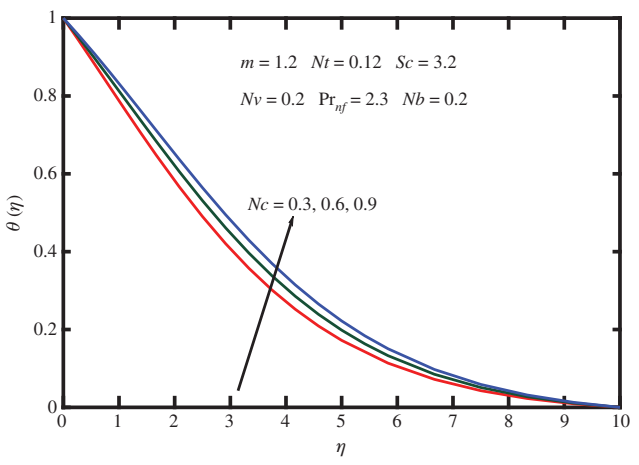


Figure 5: Temperature profiles for variable thermal conductivity parameter *Nc*.

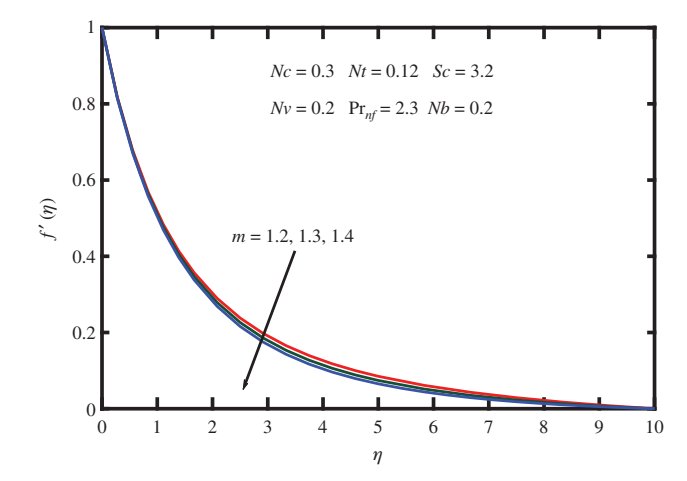


Figure 4: Velocity profiles for rheological parameter m.

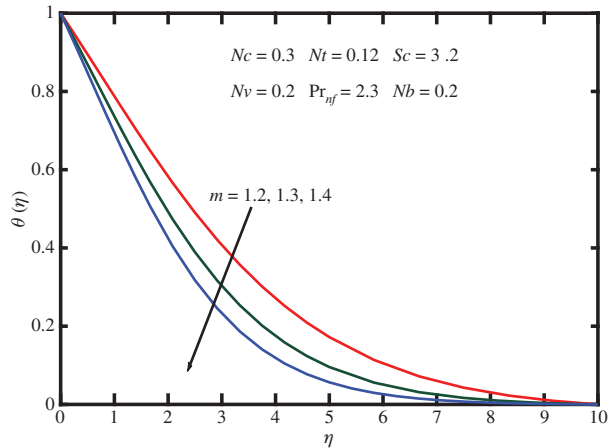


Figure 6: Temperature profiles for rheological parameter m.

thus, the thickness of the temperature boundary layer decreases.

Figure 7 portrays that Schmidt number *Sc* has a great influence on concentration boundary layer. The thickness of the concentration boundary layer decreases apparently with the enhancement of Schmidt number. This is because the higher value of *Sc* boosts the viscosity of nanofluid and reduces the Brownian motion coefficient of nanoparticles. Due to that reason, the diffusion of nanoparticles is hindered, and the thickness of concentration boundary layer is reduced. Figure 8 is similar to Figure 6, which shows that the decrease of fluidity also leads to the changes in concentration boundary layer.

The above results imply that if we want to enhance the heat transfer efficiency of the fluid, we need to make the Nc as large as possible and the m as small as possible within the desirable ranges.

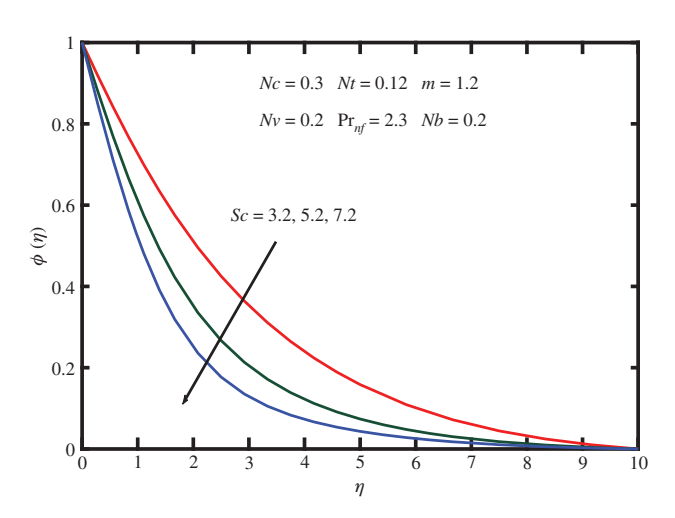


Figure 7: Concentration profiles for Schmidt number Sc.

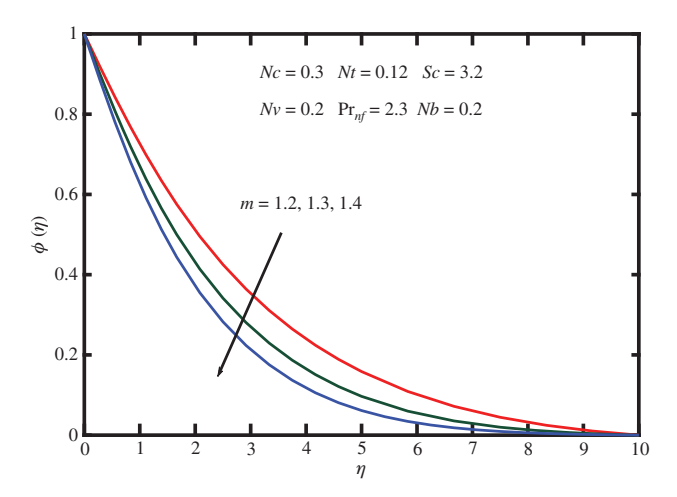


Figure 8: Concentration profiles for rheological properties parameter *m*.

5.2 The Effects of Different Parameter Values Such as Nt, U_L/U_0 , m, and Nv on Reduced Nusselt Number (Nur), Skin-Friction Coefficient (Cfr), and Sherwood Number (Shr) at the Stretching Distance L

Figures 9a and b and 10a and b show the effects of thermophoresis parameter Nt, rheological properties parameter m and drawing velocity ratio U_L/U_0 on reduced Nusselt number and reduced Sherwood number for Nb=0.2, $Pr_{nf}=2.3$, Sc=3.2, Nc=0.3, Nv=0.2, and $L/h_0=5$. Figure 11 presents the effects of drawing velocity ratio U_L/U_0 and variable viscosity parameter Nv on reduced skin-friction coefficient.

It can be seen from Figures 9a and b and 10a and b that the reduced Nusselt number and Sherwood number decrease with the increase of thermophoresis parameter *Nt* when rheological properties parameter *m* and the drawing velocity ratio U_L/U_0 are fixed. And the influence of thermophoresis parameters Nt on reduced Sherwood number is much greater than the reduced Nusselt number. In addition, the reduced Nusselt number and Sherwood number increase significantly with the enhancements of rheological properties parameter m and drawing velocity ratio U_L/U_0 . As the generalised Reynolds number is related to the rheological properties parameter m, the stronger drawing velocity ratio U_L/U_0 enhances convective heat transfer and convective mass transfer while it decays the heat conduction and mass diffusion when *m* is determined. On the other hand, the effect of Nt on convective heat and mass transfer is opposite to that of U_L/U_0 when *m* is determined.

Figure 11 describes that the absolute value of the reduced skin-friction coefficient increases sharply with the enhancement of the drawing velocity ratio for smaller drawing velocity ratio U_L/U_0 . However, when the drawing velocity ratio is relatively high, the absolute value of the reduced skin-friction coefficient increases slowly with the enhancement of the drawing velocity ratio. When the drawing velocity ratio U_L/U_0 is fixed, the larger value of variable viscosity parameter Nv enhances the absolute value of reduced skin-friction coefficient. The greater the value of U_L/U_0 is, the faster the change of absolute value of reduced skin-friction coefficient with Nv is. This is because the higher value of Nv corresponding to high viscosity fluid, resulting in an increase in the absolute value of skin-friction coefficient. On the other hand, the larger value of U_L/U_0 boosts the extensional viscosity of the thin liquid film; thus, the absolute value of the skin-friction coefficient enhances.

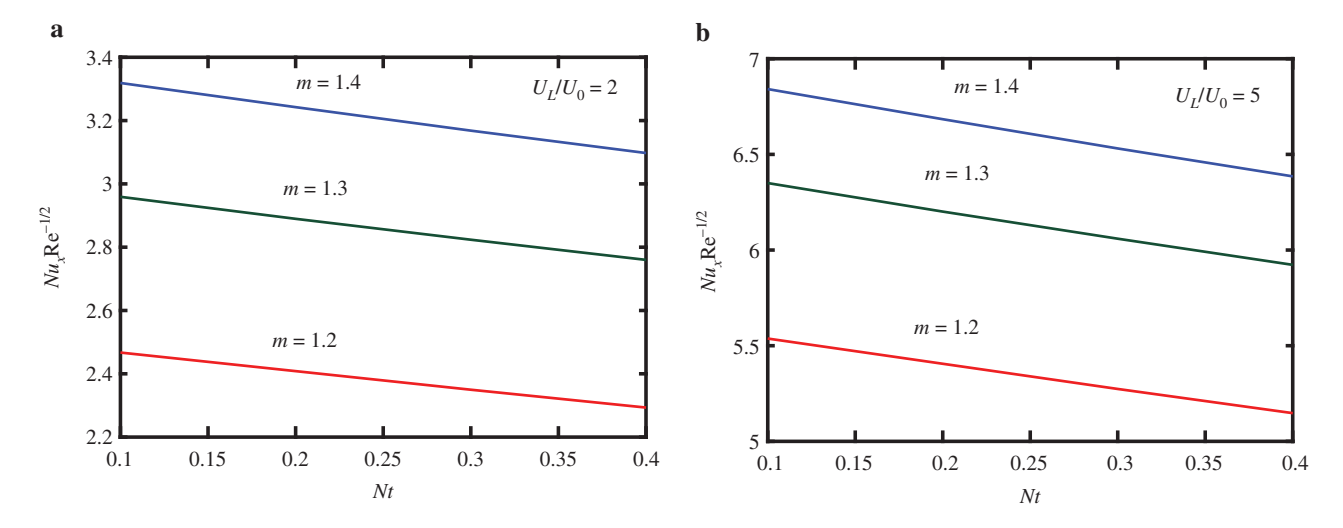


Figure 9: Influence of Nt on reduced Nusselt number under different rheological properties parameter m and drawing velocity ratio U_L/U_0 .

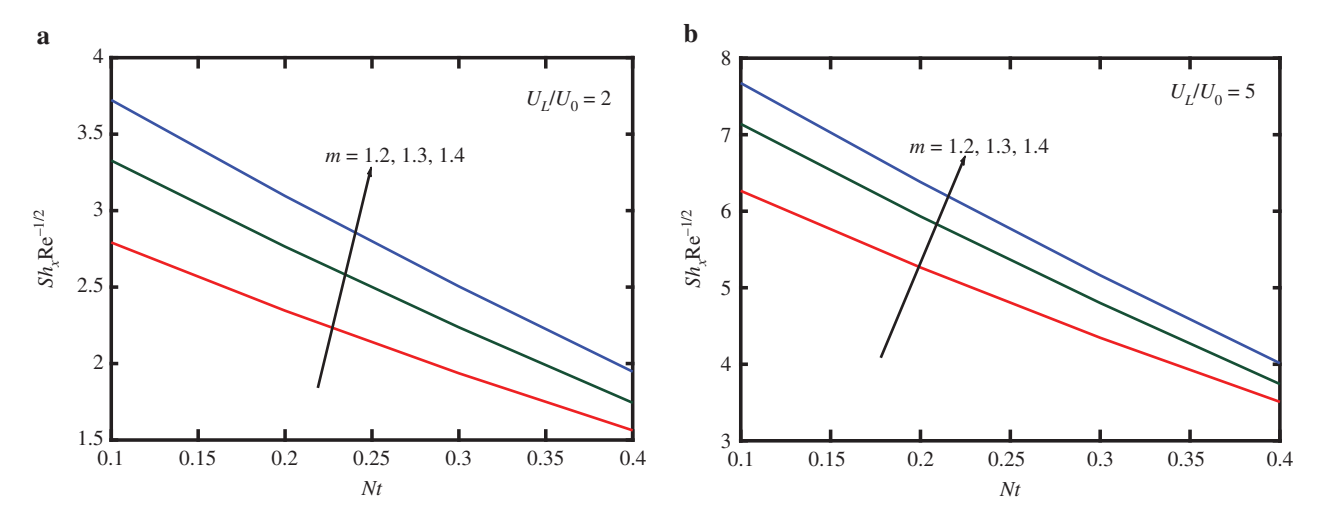


Figure 10: Influence of the Nt on reduced Sherwood number under different rheological properties parameter m and drawing velocity ratio U_L/U_0 .

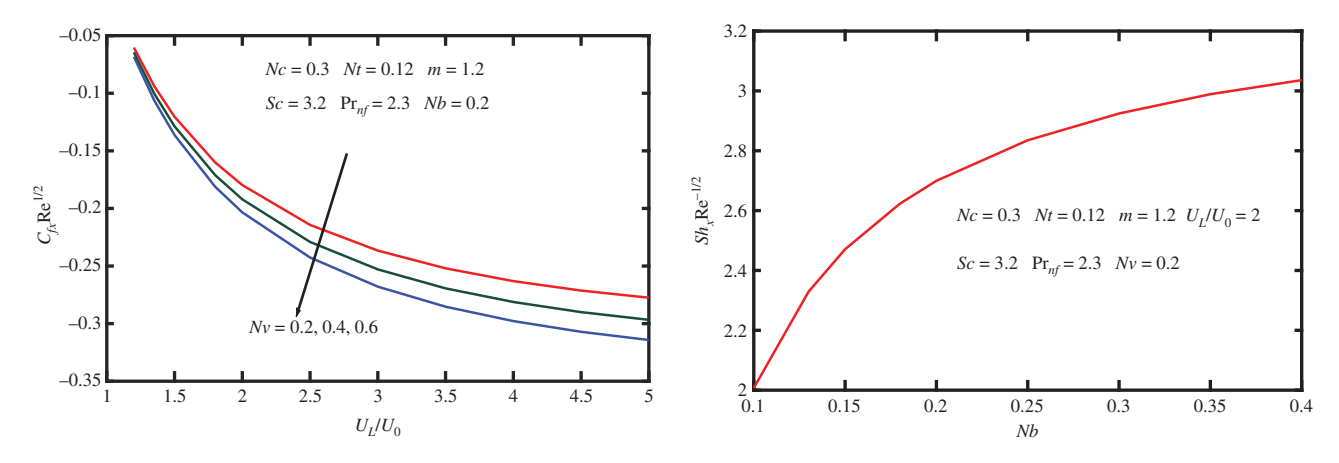


Figure 11: Influence of U_L/U_0 on the reduced skin-friction coefficient under different variable viscosity parameter Nv.

Figure 12: Influence of Brownian motion parameter Nb on the reduced Sherwood number.

5.3 The Effect of Brownian Motion Parameter Nb on the Reduced **Sherwood Number**

The relationship between Nb and the reduced Sherwood number is observed in Figure 12. It can be seen that an increase in Brownian motion parameter Nb results in the increase of the reduced Sherwood number when other parameters are fixed, whereas the smaller the Nb, the faster the reduced Sherwood number increases. This indicates that convective mass transfer is enhanced and mass diffusion is decayed for stronger Brownian motion.

6 Conclusions

The boundary-layer flow of the nanofluids induced by the motion of a thin liquid film is analysed. It is supposed that the film is incompressible and has a power-law tensile property. The coupling interface dynamics between the thin film and nanofluids (based on a Newtonian fluid) is considered, and the Brownian motion and thermophoresis in seven slip mechanisms of the nanofluid are also considered. At low concentration, the thermal conductivity and viscosity of nanofluids are linearly related to the concentration of nanoparticles. The effects of different parameters such as variable viscosity parameter Nv, variable thermal conductivity parameter Nc, Schmidt number Sc, and rheological properties parameter *m* (power-law exponent) on fields of velocity, temperature, and concentration are analysed. In addition, the effects of different parameters on the reduced Nusselt number, skin-friction coefficient, and Sherwood number are also analysed. The results are summarised as follows:

- Rheological properties parameter (power-law exponent m) and variable viscosity parameter Nv have slight effects on velocity boundary layer.
- Higher value of *Nc* enhances the temperature boundary layer thickness; however, opposite behaviour is examined via larger m.
- (iii) The function relationships between the reduced Nusselt number, Sherwood number, and thermophoresis parameter Nt are affected by rheological properties parameter (power-law exponent *m*) and drawing velocity ratio U_L/U_0 .
- (iv) Larger values of Nv and U_L/U_0 boost the reduced skin-friction coefficient.
- Stronger Brownian motion enhances the convective mass transfer.

7 Highlights

- 1. Boundary layer mechanism of a nanofluid subject to coupled interface dynamics of fluid/film is studied.
- Thermal conductivity and dynamic viscosity are assumed to be linear functions of nanoparticle concentration.
- 3. Influence of Brownian motion and thermophoresis on heat and mass transport of nanofluid are also consid-
- 4. Boundary layer behaviour strongly depends on rheological parameter of thin liquid film and velocity ratio.
- 5. Combined effects of involved parameters on boundary characteristics are also analysed in detail.

Acknowledgements: This work is supported by the National Natural Science Foundations of China (nos. 11772046, 81870345) and by the Qatar National Research Fund Grant NPRP 8-028-1-001.

Nomenclature

- transverse velocity, m/s axial velocity, m/s
- transverse and axial coordinate, respectively, m
- temperature, K
- nanoparticle concentration
- thermal conductivity, W/(m K).
- specific heat capacity, J/(kg K)
- D_B Brownian motion coefficient, m²/s thermophoretic diffusion coefficient, m²/s D_T
- half-thickness of the thin liquid film, m
- U velocity of the thin liquid film, m/s
- $N\nu$ variable viscosity parameter
- variable thermal conductivity parameter Nc
- power-law index m
- length of the thin liquid film, m
- f dimensionless stream function
- dimensionless function
- Re generalised Reynolds number
- Pr Prandtl number
- Nh Brownian motion parameter
- thermophoresis parameter Nt
- Schmidt number Sc
- Nu_x local Nusselt number
- Sh_x local Sherwood number
- local skin-friction coefficient C_{fx}
- Nur the reduced Nusselt number
- the reduced skin-friction coefficient Cfr
- the reduced Sherwood number Shr
- q_w surface heat flux
- surface mass flux

Greek symbols

- apparent viscosity coefficient, (Pa s) μ
- density, kg/m³

density of the thin liquid film, kg/m³ ρ_s

constant μ_{tf}

similarity variable n

 $\dot{\theta}$ dimensionless temperature

φ rescaled nanoparticle concentration

β, constant γ, ε

thermal diffusivity, m²/s α

kinematic viscosity of the fluid, m²/s

τ ratio between the effective heat capacity of the

nanoparticle material and heat capacity of the fluid

surface shear stress, Pa $\tau_{nf,w}$

Subscripts

0 value at coordinate origin (i.e. at x = 0, y = 0)

value at infinity (i.e. $y \rightarrow \infty$) ∞

value on the surface of the thin liquid film (i.e. y = h(x)) w

nanofluids nf nanoparticles

bf base fluid

References

- [1] B. C. Sakiadis, AIChE J. 7, 26 (1961).
- [2] F. K. Tsou, E. M. Sparrow, and R. J. Goldstein, Int. J. Heat Mass Transf. 10, 219 (1967).
- [3] S. J. Liao, J. Fluid Mech. 488, 189 (2003).
- [4] L. J. Crane, Z. Angew. Math. Phys. 21, 645 (1970).
- [5] K. R. Rajagopal, T. Y. Na, and A. S. Gupta, Rheol. Acta 23, 213 (1984).
- [6] R. S. R. Gorla, V. Dakappagari, and I. Pop, Z. Angew. Math. Mech. 75, 389 (1995).
- [7] A. Kumar, V. Sugunamma, N. Sandeep, J. Non-Equil. Thermody. 43, 327 (2018).
- [8] K. A. Kumar, J. V. R. Reddy, V. Sugunamma, and N. Sandeep, Alex. Eng. J. 57, 435 (2018).
- [9] E. Magyari and B. Keller, J. Phys. D Appl. Phys. 32, 577 (1999).
- [10] A. Kumar, V. Sugunamma, and N. Sandeep, J. Non-Equil. Thermody. 44, 101 (2019).
- [11] S. Liao, Stud. Appl. Math. 117, 239 (2006).
- [12] M. Sajid and T. Hayat, Int. Commun. Heat Mass 35, 347 (2008).
- [13] S. U. S. Choi and J. A. Estman, ASME Publ. Fed. 231, 99 (1995).
- [14] Y. Hwang, J. K. Lee, J. K. Lee, Y-M. Jeong, S. Cheong, et al., Powder Technol. 186, 145 (2008).
- [15] M. M. Rashidi, M. Nasiri, M. S. Shadloo, and Z. Yang, Heat Transfer Eng. 38, 853 (2017).
- [16] E. Sani, N. Papi, L. Mercatelli, and G. Żyła, Renew. Energy 126, 692 (2018).
- [17] K. Zaimi, A. Ishak, and I. Pop, PLoS One 9, e111743 (2014).

- [18] M. H. Fard, M. N. Esfahany, and M. R. Talaie, Int. Commun. Heat Mass 37, 91 (2010).
- [19] M. Akbari, N. Galanis, and A. Behzadmehr, Int. J. Therm. Sci. 50, 1343 (2011).
- [20] A. Behzadmehr, M. Saffar-Avval, and N. Galanis, Int. J. Heat Fluid Fl. 28, 211 (2007).
- [21] J. Buongiorno, J. Heat Transf. 128, 240 (2006).
- [22] W. A. Khan and I. Pop, Int. J. Heat Mass Tran. 53, 2477 (2010).
- [23] A. Noghrehabadi, R. Pourrajab, and M. Ghalambaz, Int. J. Therm. Sci. 54, 253 (2012).
- [24] A. Kumar, V. Sugunamma, N. Sandeep, et al., Multidisc. Model. Mater. Struct. 15, 103 (2019).
- [25] H. Zargartalebi, M. Ghalambaz, A. Noghrehabadi, and A. Chamkha, Adv. Powder Technol. 26, 819 (2015).
- [26] N. S. Akbar, D. Tripathi, Z. H. Khan, and O. A. Bég, Chem. Phys. Lett. 661, 20 (2016).
- [27] T. T. Al-Housseiny and H. A. Stone, J. Fluid Mech. 706, 597
- [28] D. M. Binding and K. Walters, J. Non-Newton. Fluid 30, 233 (1988).
- [29] H. I. Andersson, J. B. Aarseth, and B. S. Dandapat, Int. J. Heat Mass Tran. 43, 69 (2000).
- [30] B. S. Dandapat, B. Santra, and H. I. Andersson, Int. J. Heat Mass Tran. 46, 3009 (2003).
- [31] C. Y. Wang, Q. Appl. Math. 48, 601 (1990).
- [32] N. Sandeep and A. Malvandi, Adv. Powder Technol. 27, 2448 (2016).
- [33] N. Sandeep, Adv. Powder Technol. 28, 865 (2017).
- [34] R. A. Meyer, R. S. Meyer, and J. J. Green, J. Biomed. Mater. Res. A 103, 2747 (2015).
- [35] K. Sadik and A. Pramuanjaroenkij, Int. J. Heat Mass Tran. 52, 3187 (2009).
- [36] K. Khanafer and K. Vafai, Int. J. Heat Mass Tran. 54, 4410 (2011).
- [37] N. Bachok, A. Ishak, and I. Pop, Int. J. Heat Mass Tran. 55, 642 (2012).
- [38] X. Liu, L. Zheng, G. Chen, and L. Ma, J. Heat Transf. 141, 061701 (2019).
- [39] M. Chandrasekar, S. Suresh, and A. C. Bose, Exp. Therm. Fluid Sci. 34, 210 (2010).
- [40] W. Duangthongsuk and S. Wongwises, Exp. Therm. Fluid Sci. 33, 706 (2009).
- [41] M. H. Esfe, S. Saedodin, and M. Mahmoodi, Exp. Therm. Fluid Sci. 52, 68 (2014).
- [42] D. K. Agarwal, A. Vaidyanathan, and S. S. Kumar, Appl. Therm. Eng. 60, 275 (2013).
- [43] L. Godson, B. Raja, D. M. Lal, and S. Wongwises, Exp. Heat Transfer 23, 317 (2010).
- [44] A. V. Kuznetsov and D. A. Nield, Int. J. Therm. Sci. 49, 243
- [45] D. A. Nield and A. V. Kuznetsov, Int. J. Heat Mass Tran. 52, 5792 (2009).
- [46] M. Mustafa, J. A. Khan, T. Hayat, and A. Alsaedi, Int. J. Nonlinear Mech. 71, 22 (2015).